scientific reports

Check for updates

OPEN

Hedyotis diffusae herba -Scutellaria Barbata herba drug pair suppresses prostate cancer by inducing apoptosis

Junfeng Qiu[1,2,5], Litong Wu[1,2,5], Zhiming Hong[1,5], Yahong Shi[3], Yi Wei[1,2], Quan Wang[1], Zilong Chen[1], Weitian Chen[1], Qing Zhang[4], Xujun J. You[4]✉, Wenbin B. Zhou[1]✉ & Wenban Zhou[1]

Prostate cancer (PCa), a globally prevalent male malignancy, necessitates breakthroughs in treating its hormone-refractory stage. The Traditional Chinese Medicine drug pair Hedyotis Diffusae Herba – Scutellaria Barbatae Herba (HDH–SBH) shows significant antitumor value, but its multi-component synergistic mechanisms remain unclear. This study elucidated HDH-SBH's molecular mechanisms in suppressing PCa via apoptosis pathways. Network pharmacology predicted active components (quercetin, ursolic acid, apigenin) and core targets (AKT1, BCL2, NFKB) enriched in apoptosis ($P < 0.05$). Molecular docking revealed strong binding (e.g., ursolic acid-AKT1: -7.76 kcal/mol), confirmed by stable 100 ns molecular dynamics simulations (RMSD < 5.0 Å). In vitro, HDH-SBH significantly inhibited PC-3 cell proliferation (48 h IC_{50} = 1.094 mg/mL), reduced migration (36 h rate decreased by 64.2%), and induced apoptosis (rate 13.57% vs. control 4.79%). It downregulated BCL2 and p-65 protein expression ($P < 0.05$) while suppressing AKT1 phosphorylation. Thus, HDH-SBH targets the AKT1/BCL2/NFKB axis to regulate apoptosis and suppress PCa progression, providing a theoretical and experimental foundation for modernizing TCM in antitumor research.

Keywords Prostate cancer, Hedyotis diffusae herba, Scuttellaria barbatae herba, PC-3, Apoptosis, Network pharmacology

Prostate cancer (PCa), a highly prevalent malignancy of the male genitourinary system, imposes an escalating global disease burden. According to the latest *GLOBOCAN 2022 cancer statistics* published in 2024, PCa has become the second most common cancer in men worldwide and ranks fifth in global male cancer-related mortality[1,2]. Notably, epidemiological trends in China reveal a dramatic surge in PCa incidence, with statistics from the National Cancer Center indicating it as the fastest-growing male malignancy over the past decade, posing a critical public health challenge[3]. Advanced-stage PCa, particularly castration-resistant prostate cancer (CRPC), is characterized by aggressive metastasis, invasiveness, and drug resistance, directly contributing to shortened survival and diminished quality of life[4]. Clinical observations demonstrate that while androgen deprivation therapy (ADT) provides short-term disease control, most patients ultimately develop hormone-independent tumors, leading to irreversible distant metastasis and poor prognosis[5]. Although novel antiandrogens have improved survival outcomes, limitations persist in androgen receptor pathway-targeted therapies due to heterogeneous patient responses[6]. Thus, exploring innovative strategies to overcome current therapeutic bottlenecks holds urgent clinical significance.

In the modernization of traditional medicine, the antitumor mechanisms of traditional Chinese medicine (TCM) have gained increasing international attention. TCM interventions based on the *Fu Zheng Qu Xie* (supporting healthy qi and eliminating pathogens) theory not only alleviate adverse effects of chemo/

[1]Department of Andrology, Shenzhen Traditional Chinese Medicine Hospital, Shenzhen 518033, People's Republic of China. [2]Department of Andrology, The Fourth Clinical Medical College of Guangzhou, University of Chinese Medicine, Shenzhen 518033, People's Republic of China. [3]Institute of Medicinal Plant Development, Peking Union Medical College, Chinese Academy of Medical Sciences, Beijing 100193, People's Republic of China. [4]Department of Andrology, Shenzhen Bao'an Traditional Chinese Medicine Hospital Group, Guangzhou University of Chinese Medicine, Shenzhen 518100, People's Republic of China. [5]Junfeng Qiu, Litong Wu and Zhiming Hong contributed equally to this work. ✉email: youxujun90@gzucm.edu.cn; zwb1054@gzucm.edu.cn

radiotherapy but also exhibit unique advantages in modulating the tumor microenvironment and reversing drug resistance[7–9]. The drug pair *Hedyotis Diffusae Herba* (HDH) and *Scutellaria Barbatae Herba* (SBH) — a classic antitumor combination in TCM — warrants in-depth investigation for its synergistic mechanisms. HDH, derived from the dried whole plant of *Hedyotis diffusa* (Rubiaceae), is characterized by its cool nature, bitter flavor, and affinity for the stomach and large intestine meridians. It is traditionally used to clear heat, resolve toxicity, and reduce dampness-induced abscesses. Modern pharmacology confirms its antitumor effects via suppression of tumor angiogenesis and induction of apoptosis through NF-κB and PI3K/AKT signaling pathways[10,11]. SBH, obtained from the dried whole plant of *Scutellaria barbata* (Lamiaceae), exhibits a cold nature, pungent flavor, and tropism toward the lung, liver, and kidney meridians. It is traditionally employed to clear heat, detoxify, and promote blood circulation. Studies reveal that its bioactive components exert antitumor effects by regulating cyclin-dependent proteins and pro-apoptotic factors[12,13].

TCM compatibility theory emphasizes synergistic herb pairs to achieve *Zeng Xiao Jian Du* (enhanced efficacy and reduced toxicity) through precise regulation. Modern systems biology research highlights HDH-SBH drug pair as a multi-component, multi-target network regulator, offering novel insights into complex disease therapeutics[14]. This study adopts an integrative approach: Network pharmacology constructs a "component-target-pathway" interaction network to predict key nodes of HDH-SBH drug pair against PCa. Molecular docking and dynamics simulations evaluate binding activity and stability between core HDH-SBH drug pair components and PCa targets. In vitro experiments validate regulatory effects on critical targets and signaling pathways. By bridging computational predictions with experimental validation, this paradigm systematically elucidates the molecular mechanisms of HDH-SBH drug pair against PCa, providing methodological advancements for TCM modernization. The experimental workflow of this research is presented in Fig. 1.

Results

Mass spectrometry analysis

The positive and negative ion chromatograms of HDH-SBH drug pair extracts are shown in Fig. 2. Active components were identified based on molecular weight, mass spectral fragmentation patterns, and cross-referencing with literature and the Traditional Chinese Medicine Systems Pharmacology Database and Analysis Platform (TCMSP). A total of 240 components showed database matching scores ≥ 90, with 33 achieving perfect matches (100/100). After deduplication and validation against TCMSP, 10 active components were confirmed for HDH and 18 for SBH, alongside 57 unassigned compounds (Tables 1 and 2).

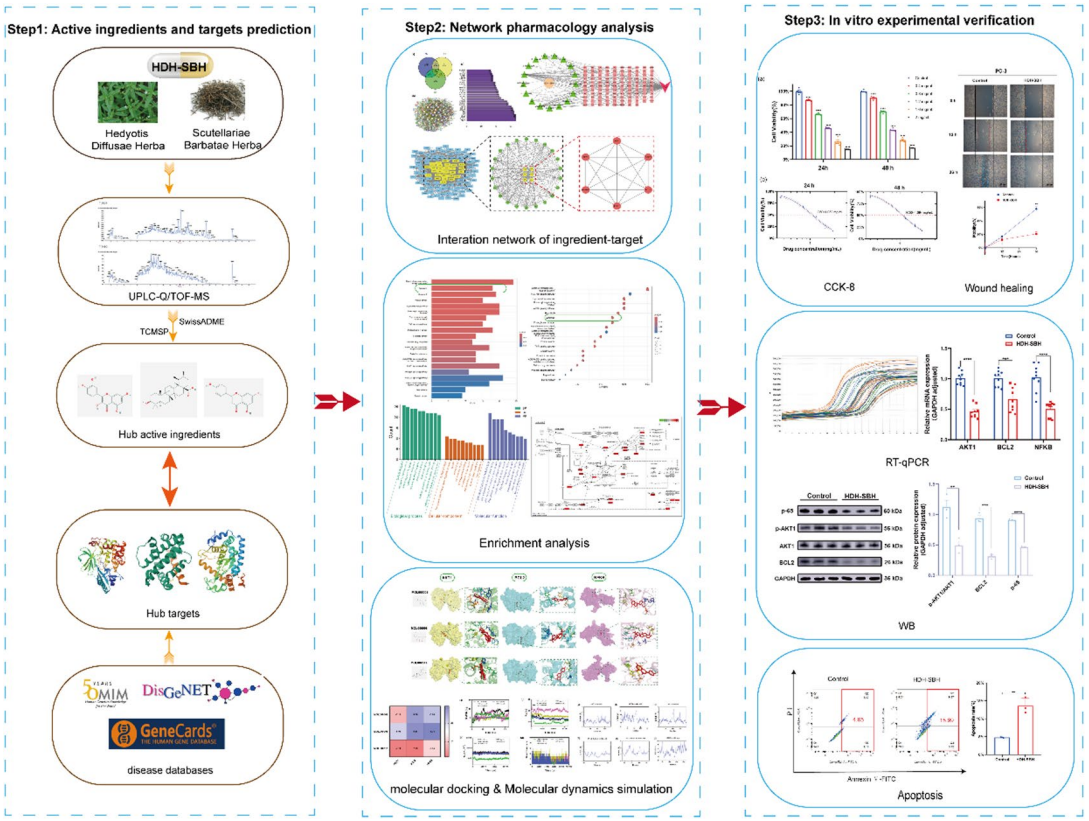

Fig. 1. The experimental workflow of this research. The OMIM icon was obtained from https://omim.org/; the DisGeNET icon from https://disgenet.com/; the GeneCards icon from https://www.genecards.org/; and the GEO icon from https://www.ncbi.nlm.nih.gov/geo/.

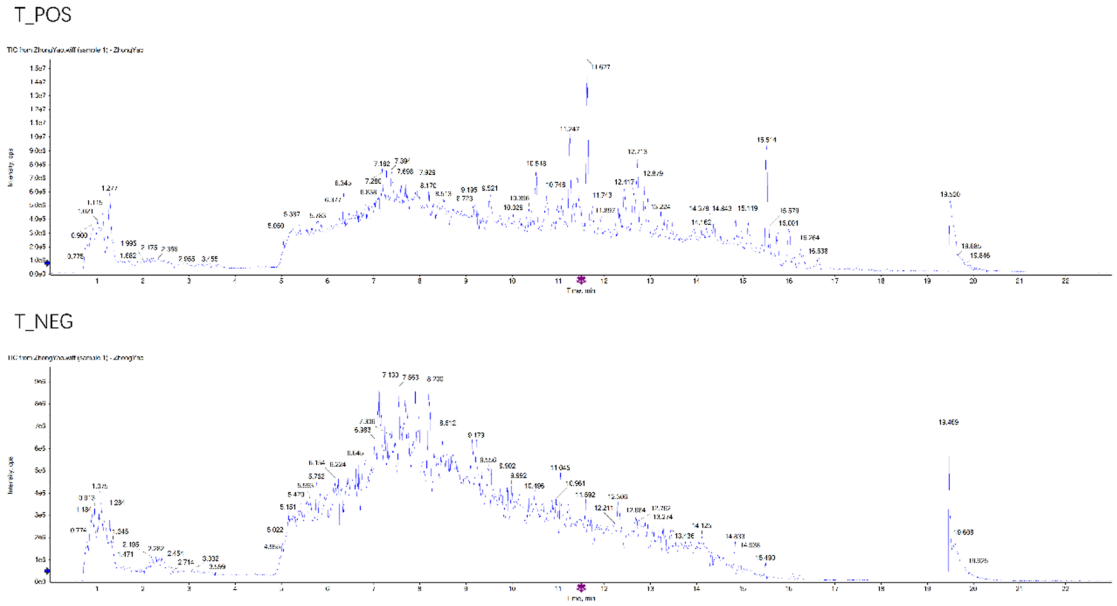

Fig. 2. Total ion chromatogram of HDH-SBH drug pair in positive and negative ion modes. (T-POS and T-NEG represent the positive ion mode and negative ion mode in mass spectrometry analysis, respectively).

No.	molecule_name	Retention time (min)	Molecular weight	Peak area	TCMSP MOL_ID
1	oleanolic acid-3-O-β-D-glucuronopyranoside_qt	14.92	456.780	64,960	MOL001655
2	(1 S,4aS,5R,7aS)−5-hydroxy-7-methylol-1-[(2 S,3R,4 S,5 S,6R)−3,4,5-trihydroxy-6-methylol-tetrahydropyran-2-yl] oxy-1,4a,5,7a-tetrahydrocyclopenta[d]pyran-4-carboxylic acid	5.02	390.380	823,100	MOL001656
3	(4aS,6aR,6aS,6bR,8aR,10R,12aR,14bS)−10-hydroxy-2,2,6a,6b,9,9,12a-heptamethyl-1,3,4,5,6,6a,7,8,8a,10,11,12,13,14b-tetradecahydropicene-4a-carboxylic acid	14.92	456.780	64,960	MOL001663
4	deacetylasperulosidic acid	5.02	390.380	823,100	MOL001664
5	succinic acid	1.61	118.100	37,330	MOL000346
6	Scopoletol	7.43	192.180	17,970	MOL000040
7	rutin	7	610.570	36,240	MOL000415
8	ursolic acid	14.92	456.780	64,960	MOL000511
9	p-coumaric acid	7.16	164.170	54,250	MOL000771
10	quercetin	8.65	302.250	20,480	MOL000098

Table 1. Main components identified from HDH.

Bioinformatics analysis

Prediction of HDH-SBH targets for PCa therapy

Integrated analysis via TCMSP, SwissTargetPrediction, and UniProt identified 94 potential targets for HDH and 116 for SBH. Disease databases (GeneCards, DisGeNET, OMIM) yielded 4,890 PCa-related targets. Venny 2.1.0 intersection revealed 108 shared targets (Fig. 3a). STRING-based PPI network analysis (confidence score > 0.4) and Cytoscape visualization (Fig. 3b) highlighted interactions among these targets. Topological analysis ranked AKT1, EGFR, ESR1, MYC, IL6, INS, CASP3, HIF1A, BCL2, and CCND1 as the top 10 core targets (Fig. 3c). CytoNCA plugin further validated centrality metrics (BC, CC, DC) for target prioritization (Fig. 4).

Component-target-disease network analysis

The interaction network of HDH-SBH drug pair active components, shared targets, and PCa was visualized using Cytoscape (Fig. 5), comprising 127 nodes (representing active components, targets, and the disease) and 233 edges. In this network, orange-red squares denote shared targets, yellow hexagons represent the HDH-SBH drug pair, green triangles indicate active components, and red V-shapes symbolize PCa. Connectivity analysis revealed that the three most interconnected components — quercetin, ursolic acid, and apigenin — exhibited the highest edge counts, establishing them as prioritized ligands for subsequent molecular docking studies. The density of edges highlighted their central roles in mediating therapeutic effects against PCa.

No.	molecule_name	Retention time (min)	Molecular weight	Peak area	TCMSP MOL_ID
1	(2R)−5,7-dihydroxy-2-(4-hydroxyphenyl)chroman-4-one	9.17	272.270	712,900	MOL001040
2	Protocatechuic acid	5.58	154.130	468,800	MOL000105
3	Vanillic acid	6.55	168.160	45,160	MOL000114
4	2',3',5,7-tetrahydroxyflavone	8.62	286.250	1,453,000	MOL012240
5	Rivularin	10.4	344.340	213,400	MOL012266
6	Baicalein	9.25	270.250	1,593,000	MOL002714
7	Scutellarein	8.2	286.250	1,446,000	MOL002737
8	Scutellarin	7.94	462.390	3,087,000	MOL002931
9	Ursolic acid	14.92	456.780	64,960	MOL000511
10	Luteolin	8.62	286.250	1,453,000	MOL000006
11	Chlorogenic acid	6.16	354.340	828,400	MOL006387
12	Oleic acid	16.23	282.520	208,900	MOL000675
13	Palmitic acid	16.09	256.480	310,300	MOL000069
14	p-coumaric acid	7.16	164.170	54,250	MOL000771
15	Apigenin	9.25	270.250	1,593,000	MOL000008
16	Stearic acid	17.21	284.540	20,520	MOL000860
17	Paeonol	9.04	166.190	35,370	MOL000874
18	Quercetin	8.65	302.250	204,800	MOL000098

Table 2. Main components identified from SBH.

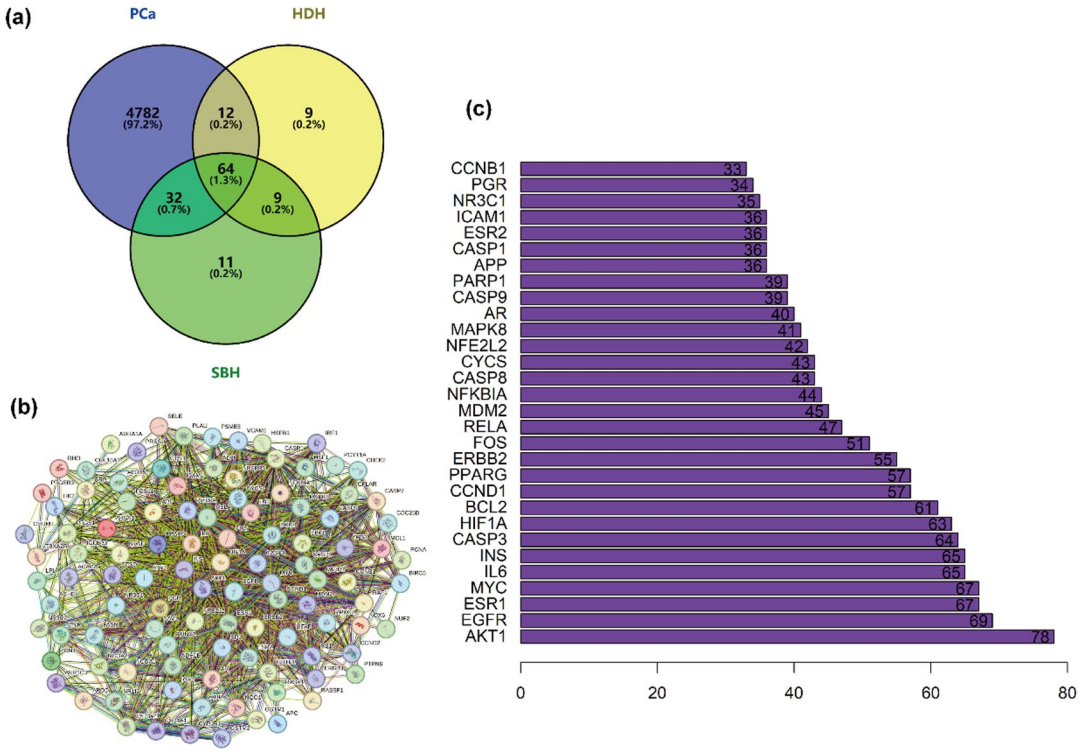

Fig. 3. Candidate targets of HDH-SBH drug pair for PCa treatment. (**a**) Venn diagram of common targets. (**b**) Protein-protein interaction network of common targets. (**c**) Association frequency histogram of common targets (The horizontal axis represents the frequency of target occurrence; higher frequencies indicate greater potential importance of the target in the HDH-SBH drug pair for PCa therapy).

GO and KEGG pathway enrichment

GO functional enrichment analysis ($P < 0.05$) identified biological processes such as gland development, oxidative stress response, and cellular response to peptides; cellular components including the nuclear envelope and RNA polymerase II transcription regulator complexes; and molecular functions like DNA-binding transcription factor activity (Fig. 6a). KEGG pathway analysis further revealed 137 enriched pathways ($P < 0.05$), with the top

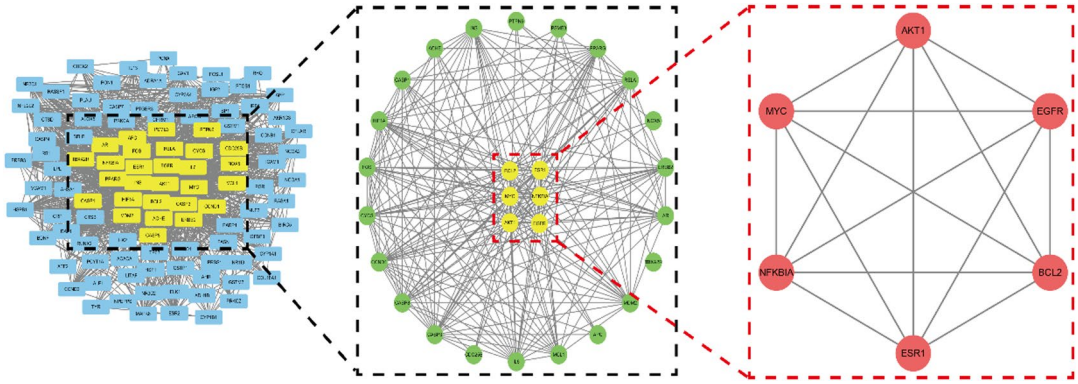

Fig. 4. Hierarchical screening network of top six targets. (Nodes represent targets, edges represent interactions between targets; more edges indicate stronger interactions.).

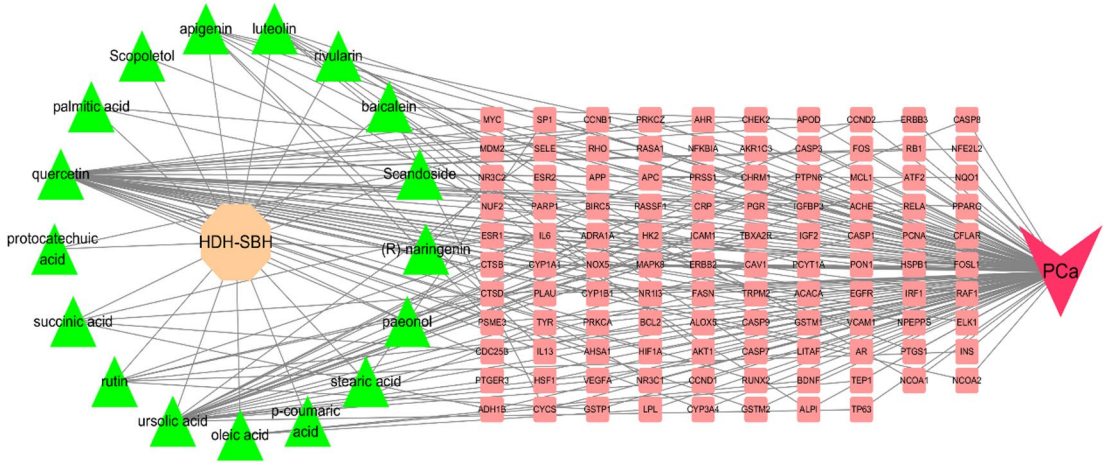

Fig. 5. Active components-common targets-disease network of HDH-SBH drug pair for PCa treatment.

20 pathways — notably apoptosis, prostate cancer, and TNF signaling — visualized in Fig. 6b. Based on network centrality metrics (BC, CC, DC) and pathway relevance, the apoptosis signaling pathway was selected as the core mechanism, with AKT1, BCL2, and NFKB (which encodes the p-65 subunit) identified as pivotal therapeutic targets (Fig. 7).

Molecular docking validation of key components and core targets

Molecular docking between the core active components (quercetin, ursolic acid, apigenin) and targets (AKT1, BCL2, NFKB) was performed using AutoDock, with binding affinity values displayed as a heatmap (Fig. 8a). Binding energies below 0 kJ/mol indicated spontaneous binding potential, while values < − 5 kcal/mol (consistent with prior studies) confirmed strong ligand-receptor interactions[15,16]. Notably, ursolic acid exhibited the strongest binding affinity with AKT1, BCL2, and NFKB (Fig. 8b), suggesting its pivotal role in mediating HDH-SBH's anti-PCa effects through these targets.

Molecular dynamics simulations

Molecular dynamics simulations revealed stable binding of HDH-SBH drug pair components to core targets, as evidenced by root mean square deviation (RMSD) values equilibrating within 4.1–8.9 Å after 10–98 ns for all complexes (e.g., AKT1-apigenin at 4.8 Å post-10 ns; AKT1-ursolic acid at 8.9 Å post-90 ns), alongside minor fluctuations in radius of gyration (Rg) and solvent-accessible surface area (SASA), indicative of controlled conformational changes (Fig. 9a–c). Hydrogen bond analysis demonstrated sustained interactions, with AKT1-apigenin and AKT1-quercetin complexes maintaining averages of 2–3 bonds, while ursolic acid-bound systems (AKT1, BCL2, NFKB) exhibited 1–2 bonds (Fig. 9d). Low root mean square fluctuation (RMSF) values (<6 Å) across all complexes confirmed minimal residue flexibility and high structural stability (Fig. 9e–j). Notably, the AKT1-apigenin complex displayed optimal stability (lowest RMSD, consistent hydrogen bonding), validating apigenin as the most effective AKT1-targeting component within HDH-SBH. The stability of the simulations, as evidenced by the plateaued RMSD values and consistent hydrogen bonding after an initial equilibration period (typically within the first 10–20 ns), validates the reliability of the docking predictions for these complexes.

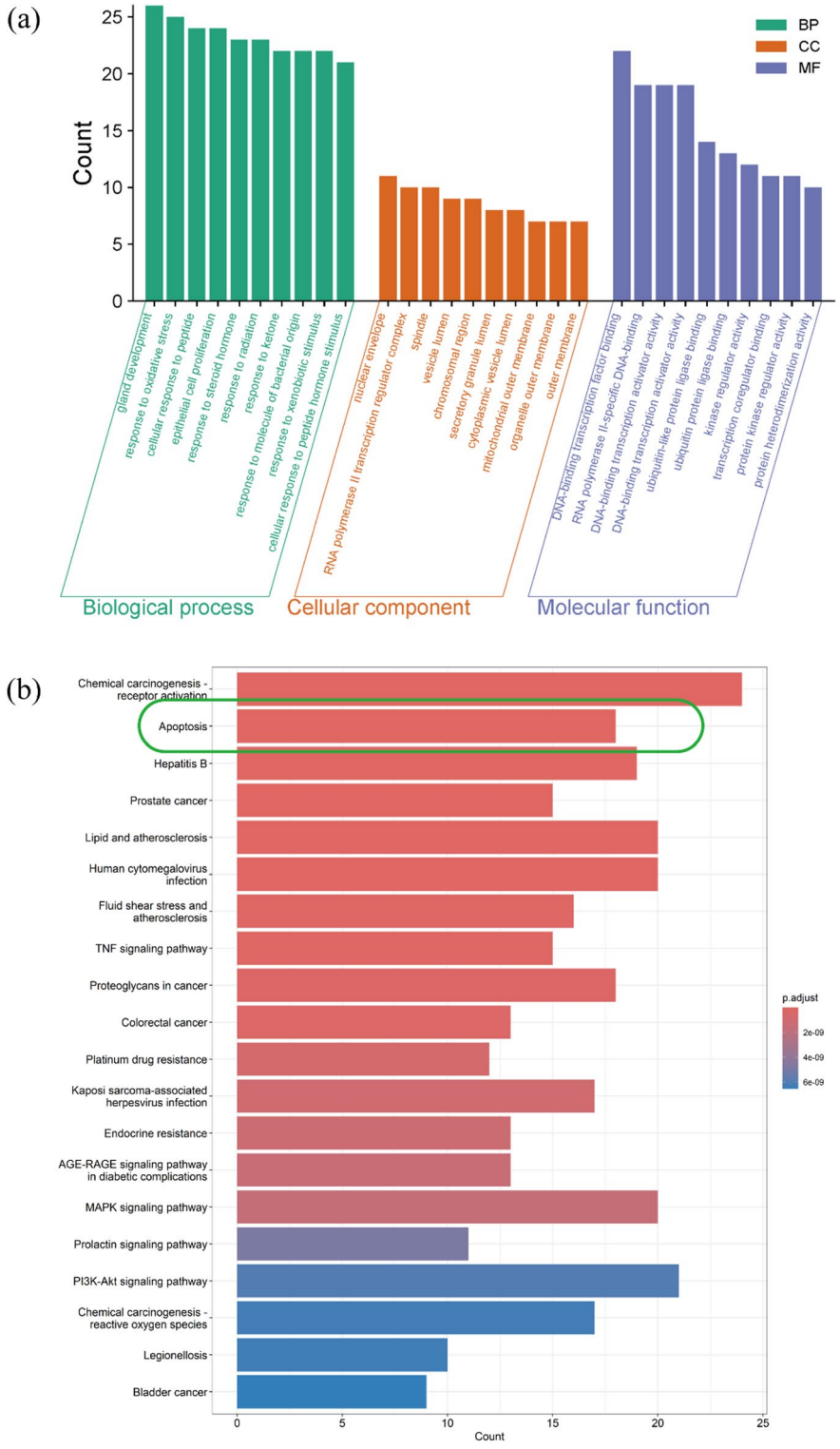

Fig. 6. (**a**) GO enrichment analysis bar chart of HDH-SBH drug pair in PCa treatment. (**b**) KEGG pathway analysis bar chart and bubble diagram of HDH-SBH drug pair in PCa treatment.

In vitro experimental validation

Cell viability assay

HDH-SBH drug pair significantly inhibited the proliferation of PC-3 cells in a concentration- and time-dependent manner. After 24 h of treatment, the IC_{50} was 1.059 mg/mL, which slightly increased to 1.094 mg/mL at 48 h ($P = 0.000 < 0.05$ vs. control group) (Fig. 10). Notably, the control group exhibited higher cell density at

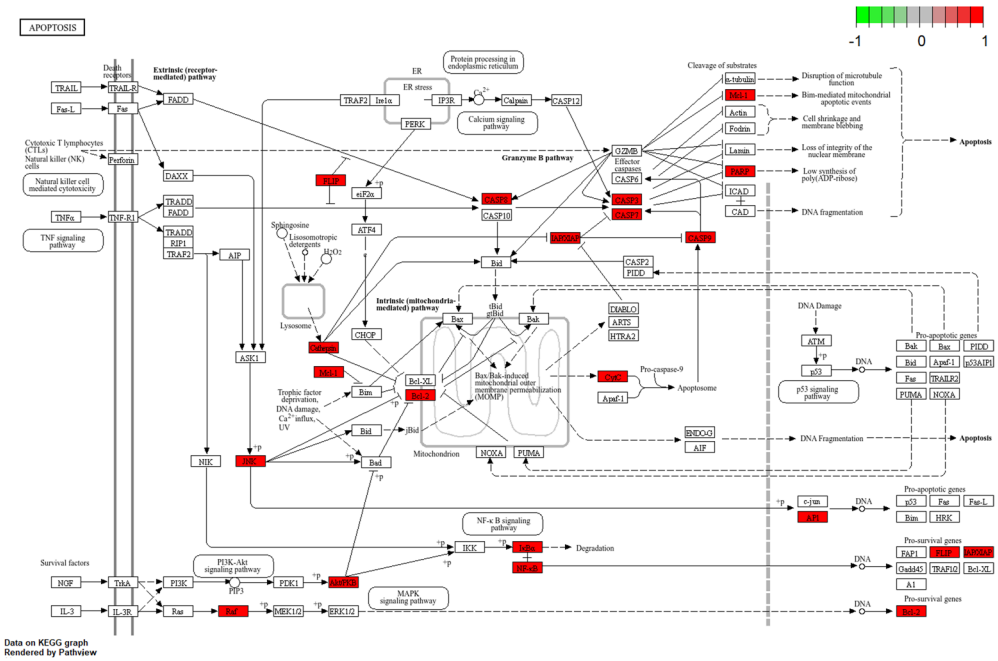

Fig. 7. Core pathway diagram of HDH-SBH drug pair in PCa treatment. (Red rectangles indicate potential therapeutic targets enriched in this study. The figure was obtained from www.kegg.jp/kegg/kegg1.html.).

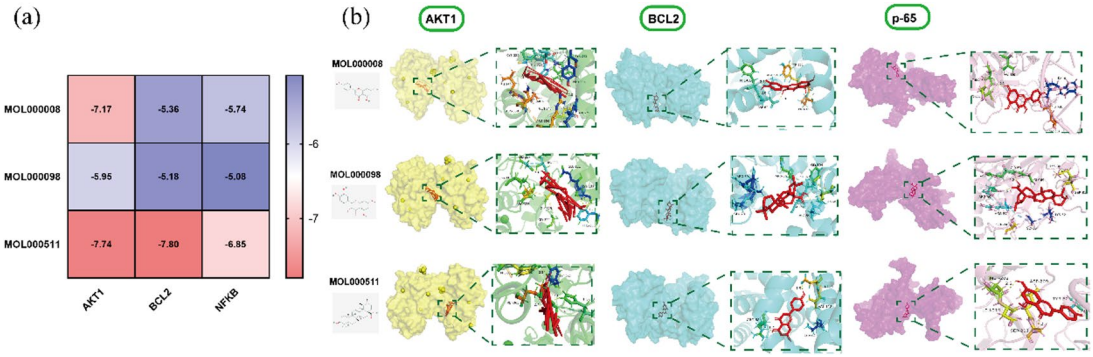

Fig. 8. (**a**) Binding energy thermogram of the four core active ingredients in HDH-SBH drug pair with the three core targets in PCa. (**b**) Docking pattern of the three core active ingredients in HDH-SBH drug pair with the three core targets in PCa.

48 h compared to 24 h, supporting the selection of the 48 h IC_{50} value (1.094 mg/mL) for subsequent experiments to ensure robust cell populations for functional assays.

Migration capacity analysis

Wound healing assays revealed that HDH-SBH drug pair suppressed PC-3 cell migration in a time-dependent manner. At 12 h post-intervention, the migration rate of the HDH-SBH group (12.07 ± 8.92%) showed no significant difference compared to the control group (16.39 ± 2.14%, $P = 0.573 > 0.05$). However, by 36 h, HDH-SBH drug pair treatment markedly reduced the migration rate to 20.67 ± 6.83%, significantly lower than the control group (57.79 ± 5.86%, $P = 0.001 < 0.05$), demonstrating delayed but potent anti-migratory effects (Fig. 11).

Core target mRNA expression analysis

qRT-PCR analysis confirmed that HDH-SBH (1.094 mg/mL) downregulated mRNA expression of apoptosis-related targets. Compared to the control group, the HDH-SBH group showed significantly reduced expression of AKT1 (0.46 ± 0.10 vs. 1.00 ± 0.00), BCL2 (0.67 ± 0.20 vs. 1.00 ± 0.00), and NFKB (0.50 ± 0.13 vs. 1.00 ± 0.00) ($P = 0.000 < 0.05$ for all), consistent with the predicted modulation of the apoptosis signaling pathway (Fig. 12).

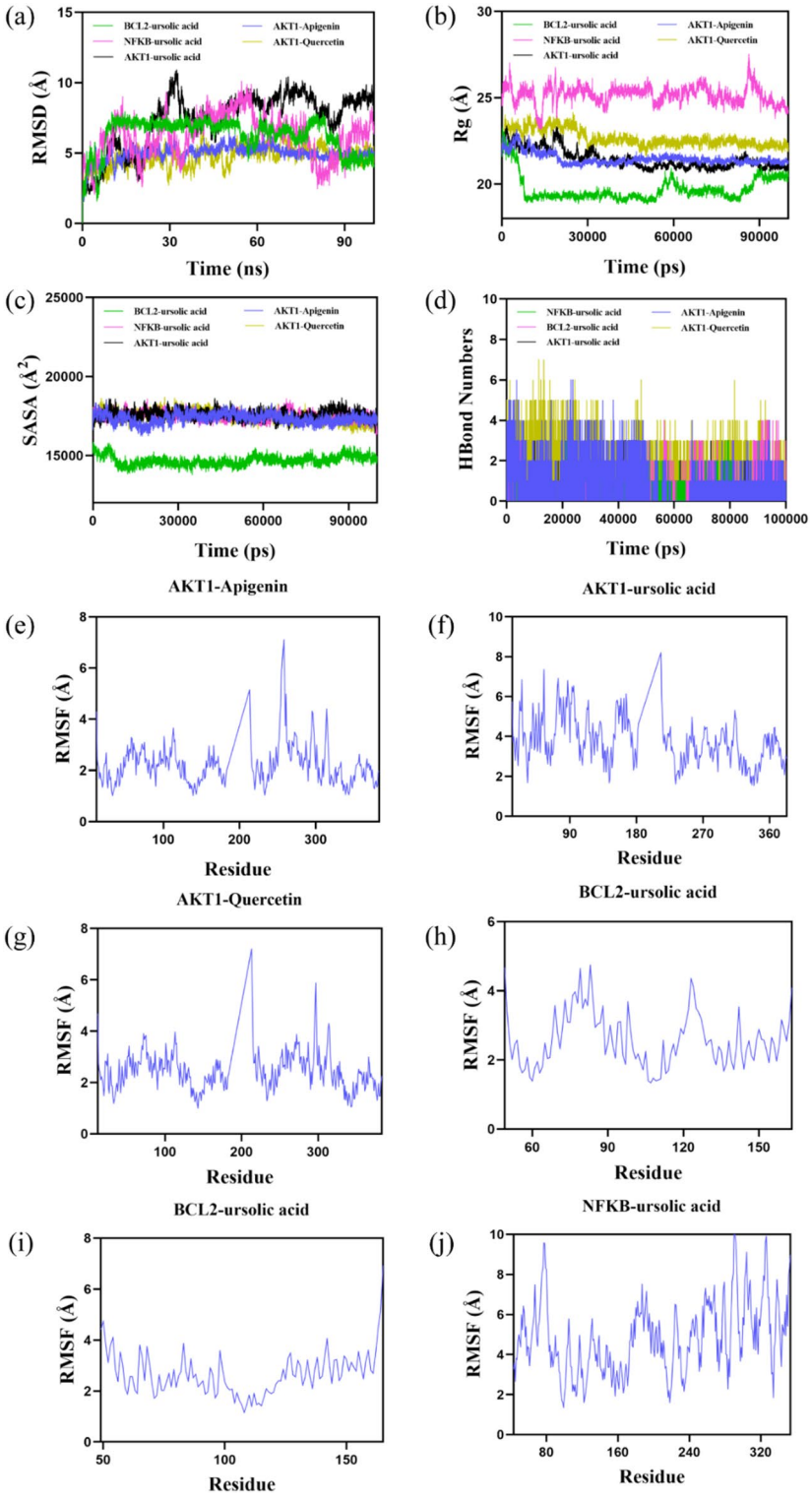

Fig. 9. Molecular dynamics simulation analysis of core component-target complexes (**a**–**d**). (**a**) Root mean square deviation (RMSD) of protein backbone. The plateau of RMSD curves after ~20 ns indicates the system reached a stable state. (**b**) Radius of gyration (Rg). (**c**) Solvent-accessible surface area (SASA). (**d**) Number of hydrogen bonds. Data for the entire 100 ns simulation are shown to fully represent the dynamic process. RMSF values of amino acid backbone atoms in protein-ligand complexes over time (**e**–**j**). (**e**) AKT1-Apigenin. (**f**) AKT1-Ursolic acid. (**g**) AKT1-Quercetin. (**h**) BCL2-chain A-Ursolic acid. (**i**) BCL2-chain B-Ursolic acid. (**j**) NFKB-Ursolic acid.

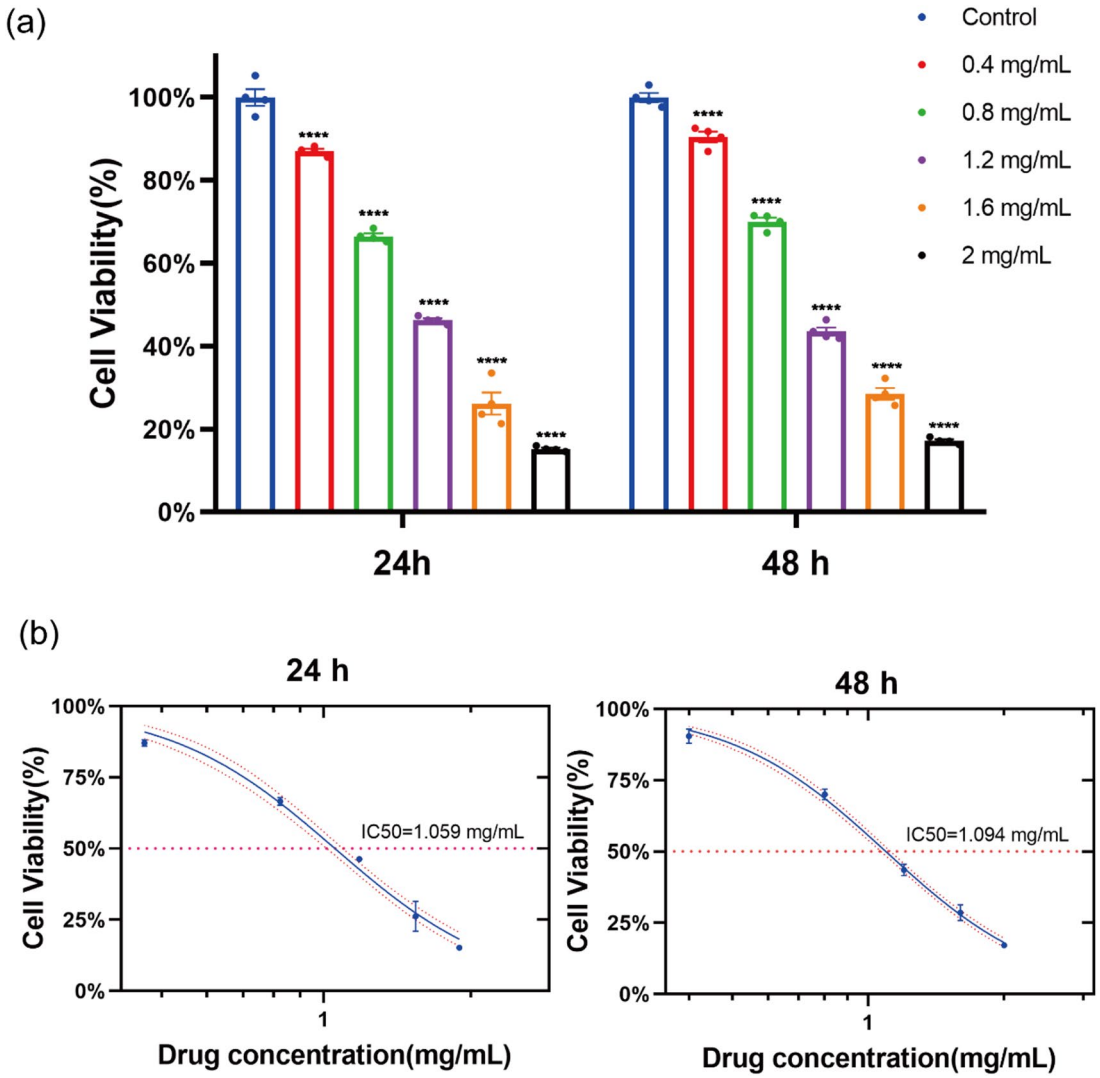

Fig. 10. HDH-SBH drug pair inhibited Proliferation in PC-3 cells. (**a**) Bar chart of viability rate of PC-3 cells treated with different concentrations of HDH-SBH drug pair intervention at two time points (Data are presented as mean ± SD ($n = 6$) and were analyzed by unpaired two-tailed Student's t test. Compared with the Control group, ****$P<0.0001$). (**b**) The 24-hour and 48-hour half inhibitory concentration of HDH-SBH drug pair on PC-3 cells. (Note: The red horizontal dashed line represents the half inhibitory concentration value, and the red curves represent the 95% confidence interval.).

Core target protein expression analysis

Western blot results demonstrated that HDH-SBH drug pair (1.094 mg/mL) significantly enhanced AKT1 phosphorylation ($P = 0.010 < 0.05$) while reducing protein levels of BCL2 ($P = 0.000 < 0.05$) and p-65 (a subunit encoded by the NFKB gene) ($P = 0.000 < 0.05$). Total AKT1 expression remained unchanged compared to the control group ($P = 0.063 > 0.05$), suggesting that HDH-SBH drug pair specifically regulates post-translational modifications rather than total protein synthesis (Fig. 13).

Apoptosis analysis

Flow cytometry revealed that HDH-SBH drug pair treatment for 48 h significantly increased the apoptosis rate of PC-3 cells (13.57 ± 2.19%) compared to the control group (4.79 ± 0.13%, $P = 0.002 < 0.05$), confirming its pro-apoptotic activity (Fig. 14).

Materials and methods

HDH-SBH drug pair mass spectrometry analysis

Extraction and Preparation of HDH-SBH

A mixture of HDH (50 g) and SBH (50 g) was added to a 2 L distillation flask with 800 mL of 70% ethanol. The selection of ethanol as the extraction solvent is consistent with its widespread use in both traditional TCM formulations and modern phytochemical research, as it efficiently extracts a broad spectrum of medium- and

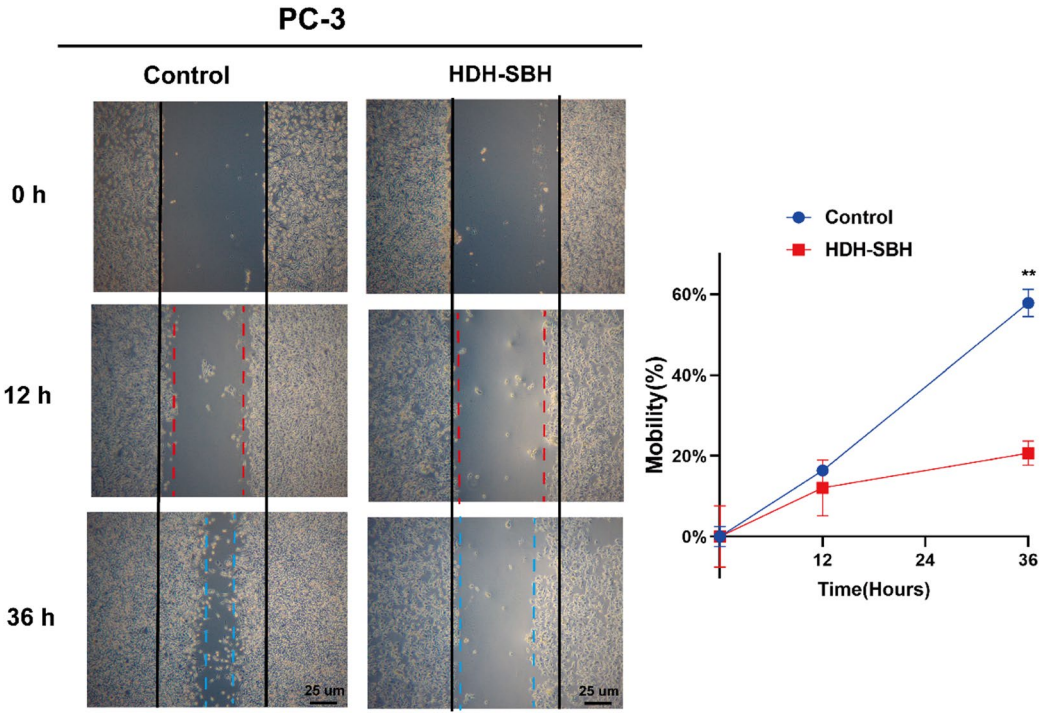

Fig. 11. The effect of HDH-SBH drug pair on PC-3 cells in wounding experiments. (Data are presented as mean ± SD ($n = 3$) and were analyzed by unpaired two-tailed Student's t test. Compared with the Control group, $^{**}P<0.01$).

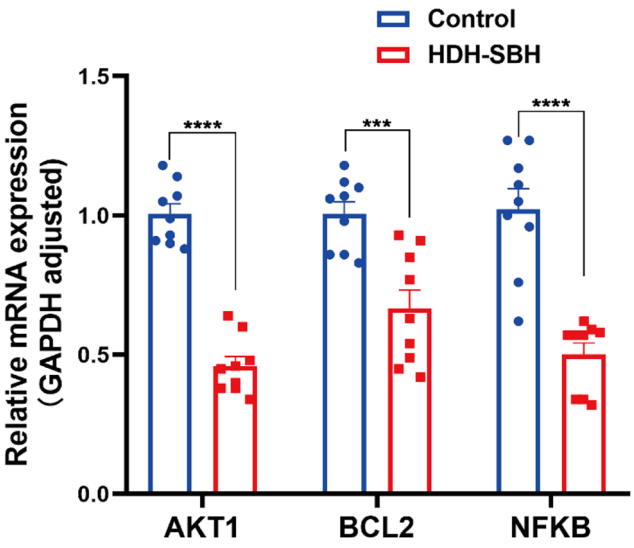

Fig. 12. The effect of HDH-SBH drug pair on mRNA expression of core targets in PC-3 cells. ((Data are presented as mean ± SD ($n = 3$) and were analyzed by unpaired two-tailed Student's t test. Compared with the Control group, $^{***}P<0.001$, $^{****}P<0.0001$).

high-polarity bioactive compounds, including the flavonoids and triterpenoids central to this study[17,18]. The flask was placed in a thermostatic water bath at 95 °C for 1 h for initial extraction. After filtration, the residue was re-extracted with 600 mL of 70% ethanol for 0.5 h under the same conditions. The combined extracts were concentrated using a rotary evaporator (60 °C, 60 rpm) until solids precipitated. The concentrate was pre-cooled at −20 °C and lyophilized in a vacuum freeze-dryer to obtain 17.75 g of freeze-dried powder (yield: 17.75% based on 100% purity). A portion of the powder was dissolved in ultrapure water to prepare a 4 mg/mL solution and sterilized by filtration through a 0.22 μm membrane.

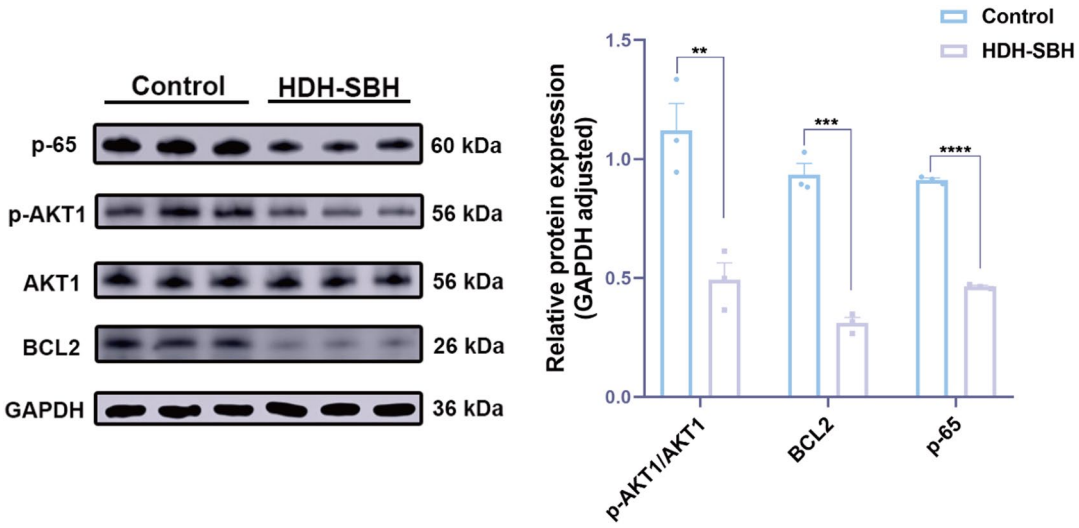

Fig. 13. The effect of HDH-SBH drug pair on protein expression of core targets in PC-3 cells. ((Data are presented as mean ± SD ($n = 3$) and were analyzed by unpaired two-tailed Student's t test. Compared with the Control group, $^{**}P<0.01$, $^{***}P<0.001$, $^{****}P<0.0001$).

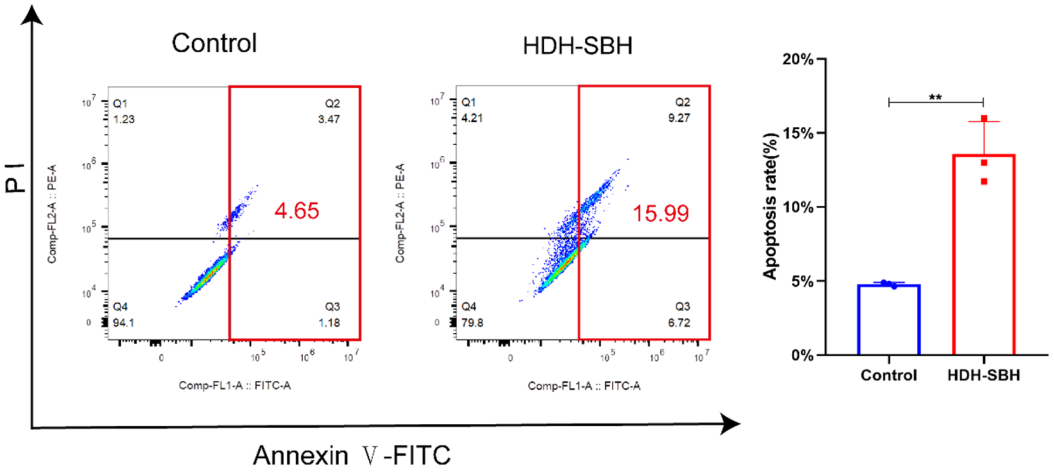

Fig. 14. The effect of HDH-SBH drug pair on PC-3 cells in apoptosis. ((Data are presented as mean ± SD ($n = 3$) and were analyzed by unpaired two-tailed Student's t test. Compared with the Control group, $^{**}P<0.01$).

Preparation of test solutions

A 100 µL aliquot of the HDH-SBH solution (50 mg freeze-dried powder dissolved in 100 mL solvent) was mixed with 400 µL methanol/acetonitrile (v/v, 1:1), vortexed for 30 s, and sonicated at 4 °C for 10 min. The mixture was incubated at −20 °C for 1 h, followed by centrifugation at 13,000 rpm (4 °C, 15 min). The supernatant was evaporated to dryness using a vacuum concentrator at 4 °C. The residue was reconstituted in 100 µL acetonitrile/water (v/v, 1:1), vortexed for 30 s, sonicated at 4 °C for 10 min, and centrifuged (13,000 rpm, 4 °C, 15 min). The final supernatant was subjected to positive and negative ion mode mass spectrometry.

Chromatographic conditions

Separation was performed on a Waters HSS T3 column (100 × 2.1 mm, 1.7 µm) with mobile phase A (0.1% formic acid in water) and mobile phase B (acetonitrile). The gradient elution program is detailed in Table 3. The flow rate was 0.3 mL/min, injection volume 3 µL, and column temperature 40 °C.

Mass spectrometry conditions

Mass spectrometry, a widely used analytical chemistry technique for identifying chemical components in traditional Chinese medicine, plays a critical role in systematically elucidating the network of pharmacological mechanisms when integrated with network pharmacology in systematic pharmacological research. Ion source: Electrospray ionization (ESI) with data-dependent acquisition. Positive ion mode: Scan range m/z 60–1000; sheath gas (N_2) temperature 550 °C; declustering voltage 80 V; collision energy 10 V; ion spray voltage 5500 V.

Time	B%
0.01	1
1.5	1
13	99
16.5	99
16.6	1
20	Stop

Table 3. Chromatography gradient elution program.

Negative ion mode: Scan range *m/z* 60–1000; sheath gas (N_2) temperature 550 °C; declustering voltage 80 V; collision energy 10 V; ion spray voltage − 4500 V.

HDH-SBH target screening

Active components identified by UPLC-Q/TOF-MS were input into the TCMSP(https://old.tcmsp-e.com/tcmsp.php) to retrieve potential therapeutic targets. Further screening was performed using SwissTargetPrediction (http://www.swisstargetprediction.ch/), followed by target standardization via UniProt (https://www.uniprot.org).

Prostate cancer target acquisition

PCa-related targets were retrieved from GeneCards (https://www.genecards.org/), DisGeNET (https://www.disgenet.org/search), and OMIM (https://omim.org/search/advanced/geneMap) using "Prostate Cancer" as the keyword. Duplicates were removed, and protein names were standardized via UniProt.

Shared target screening and PPI network construction

HDH-SBH drug pair targets and PCa disease targets were intersected using Venny 2.1.0 to generate shared targets (Venn diagram). The shared targets were input into STRING (https://string-db.org/) with species set to *Homo sapiens*, confidence threshold > 0.4, and disconnected nodes hidden. The PPI network was imported into Cytoscape 3.7.2 for topology analysis. Node size and color intensity reflected degree centrality. The top 10 targets were selected as core HDH-SBH drug pair anti-PCa targets using the MCODE plugin.

"Herb-component-target-disease" network construction

Nodes (herbs, components, targets, diseases) and edges (interactions) were compiled in Excel and visualized in Cytoscape 3.7.2. Topological parameters (degree, betweenness centrality [BC], closeness centrality [CC]) were calculated using Network Analyzer. Core components were filtered based on median BC/CC thresholds and ranked by degree value.

GO and KEGG enrichment analysis

Shared targets were analyzed via Metascape (https://metascape.org/) and Bioconductor (https://bioconductor.org/) for Gene Ontology (GO: biological processes [BP], cellular components [CC], molecular functions [MF]) and Kyoto Encyclopedia of Genes and Genomes (KEGG) pathway enrichment. Results were visualized as bar and bubble plots.

Molecular Docking validation

Core component 2D structures (SDF format) were downloaded from PubChem (https://pubchem.ncbi.nlm.nih.gov/), energy-minimized using ChemBio3D Ultra 14.0, and docked to target proteins (PDB structures from RCSB, https://www.rcsb.org/) via semi-flexible CDOCKER in PyMOL 3.0. Binding energy <−5 kcal/mol and hydrogen bond counts were used to evaluate stability.

Molecular dynamics (MD) simulation

A 100 ns MD simulation was performed using GROMACS 2022. The protein-ligand complex was parameterized with the CHARMM36 force field[19], and ligands were modeled using GAFF2. The system was solvated in a TIP3P water box[20] with periodic boundary conditions (1.2 nm). Electrostatic interactions were handled via the Particle Mesh Ewald (PME) method. After equilibration (NVT/NPT ensembles, 100 ps), production runs were conducted at 310 K and 1 bar.

In vitro experimental validation

Cell line and test materials

The human prostate cancer cell line PC-3 (poorly differentiated, purchased from Beijing Beina Biotechnology Co., China) was cultured in complete medium (F12K supplemented with 10% fetal bovine serum and 1% penicillin/streptomycin) at 37 °C under 5% CO_2. Hedyotis Diffusae Herba (HDH, batch no. A211216) and Scutellaria Barbatae Herba (SBH, batch no. A220728) were sourced from Jiangxi and Anhui provinces, respectively. Both herbs were authenticated by the Department of Pharmacy, Shenzhen Hospital of Traditional Chinese Medicine, in accordance with the Chinese Pharmacopoeia (2020 edition).

Gene	Forward primer(s) (5' to 3')	Reverse primer(s) (5' to 3')
AKT1	AGCGACGTGGCTATTGTGAAG	GCCATCATTCTTGAGGAGGAAGT
BCL2	GGTGGGGTCATGTGTGTGG	CGGTTCAGGTACTCAGTCATCC
p-65	ATGTGGAGATCATTGAGCAGC	CCTGGTCCTGTGTAGCCATT
GAPDH	ACAACTTTGGTATCGTGGAAGG	GCCATCACGCCACAGTTTC

Table 4. The primer sequences of qRT-PCR.

Component	Volume/μL
2×Taq Master Mix*	10uL
Upstream primer	1 uL
Downstream primer	1 uL
Sample	1 uL
ddH_2O	7 uL

Table 5. The qRT-PCR reaction system.

Key reagents and instruments

Reagents: Fetal bovine serum (Meisen, batch no. CTCC-002–071-500); 0.25% Trypsin-EDTA phenol red (Meisen, batch no. CTCC-002–006); F-12 K medium (Meisen, batch no. CTCC-002–007); Cell Counting Kit-8 (Biosharp, batch no. BS350B); Western blot reagents (Beyotime Biotech Inc.); AKT1 (ZENBIO, batch no. R23412); p-AKT1 (Ser473) (ZENBIO, batch no. R22961); BCL2 (Proteintech, batch no. 12789-1-AP); p-65 (Proteintech, batch no. 10745-1-AP). Instruments: DSZ2000X fluorescence microscope (Zhongxian Hengye Co., Beijing); DH-160ICO_2 incubator (Santeng Instruments, Shanghai); EIX808U microplate reader (BioTek, USA); CytoFLEX flow cytometer (Beckman Coulter, USA); DYCZ-24DH electrophoresis system and DYY-7 C transfer unit (Liuyi Biotechnology, Beijing); ChemiScope 6100 chemiluminescence imager (Qinxiang Scientific Instruments, Shanghai).

CCK-8 assay

PC-3 cells in logarithmic growth phase were seeded into 96-well plates at 6.0×10^3 cells/well (100 μL/well of complete medium). After 24 h of adhesion, cells were treated with HDH-SBH drug pair at gradient concentrations (2, 1.6, 1.2, 0.8, 0.4 mg/mL) or control medium (6 replicates per group). At 24 h and 48 h, 100 μL of CCK-8 solution (medium: reagent = 9:1) was added to each well, followed by 90 min incubation in the dark. Absorbance was measured at 450 nm (reference: 650 nm) using a microplate reader. Cell proliferation inhibition rate was calculated as: Inhibition (%) = $(OD_{control} - OD_{treatment})/(OD_{control} - OD_{blank})\times100\%$. Three independent experiments were performed to ensure reproducibility.

Wound healing assay

PC-3 cells (1.0×10^5 cells/well) were seeded into 6-well plates and cultured to 90% confluency. Uniform scratches were created using a 200 μL pipette tip aligned with a laser-etched grid (2 mm spacing). Detached cells were removed by gentle PBS washes. Cells were treated with HDH-SBH drug pair at the 48 h IC_{50} concentration (determined in CCK-8 assays) or control medium. Scratch closure was monitored at 0, 12, and 36 h using phase-contrast microscopy (4 × objective). Migration rates were quantified with ImageJ (MRI Wound Healing Tool plugin) as: Relative closure (%)= $(D_0 - D_{12/36})/D_{12/36}\times100\%$. Experiments were conducted under controlled temperature/humidity with evaporation prevention measures and triplicate repeats.

qRT-PCR

PC-3 cells (5×10^4 cells/mL) were seeded into 6-well plates and treated with HDH-SBH drug pair at the IC_{50} concentration (48 h) or control medium for 48 h. Total RNA was extracted using TRIzol, quantified via NanoDrop (A260/A280 = 1.8–2.1), and reverse-transcribed using a commercial kit. Primer sequences (Table 4) and reaction conditions (Table 5) are provided in supplementary data. GAPDH served as the internal control.

Western blotting

Cells were treated as described in Sect. 1.9.5. After 48 h of intervention, 200 μL of cell lysis buffer was added to each well, and cells were scraped on ice, transferred to 1.5 mL microcentrifuge tubes, and centrifuged at 12,000 rpm (4 °C, 15 min). Total protein was quantified using the BCA assay. Proteins were separated by SDS-PAGE, transferred to PVDF membranes, blocked with 5% non-fat milk, and incubated overnight at 4 °C with primary antibodies: AKT1 (R23412, 1:1000), p-AKT1 (Ser473) (R22961, 1:1000), BCL2 (12789-1-AP, 1:5000), p-65 (10745-1-AP, 1:3000). Membranes were washed and incubated with HRP-conjugated secondary antibody (511203, 1:10,000) for 1 h. Protein bands were visualized using chemiluminescence, and relative expression levels were quantified as target protein/GAPDH grayscale ratios using ImageJ.

Apoptosis assay

Following the Sect. 1.9.5 protocol, cells were treated for 48 h. Suspended cells from the supernatant and adherent cells (detached with 0.25% trypsin-EDTA, 37 °C, 2 min) were pooled and centrifuged (400×*g*, 4 °C). After washing with ice-cold PBS, cells were resuspended in 490 µL binding buffer, stained with 5 µL Annexin V-FITC and 5 µL propidium iodide (PI), and incubated in the dark for 15 min. Flow cytometry (CytoFLEX) was performed within 30 min post-staining. Apoptotic populations were quantified using a two-parameter scatter plot (FITC vs. PI). Three independent replicates were conducted.

Data analysis

All data were processed using SPSS 26.0 and visualized with GraphPad Prism 8.0, with continuous variables expressed as mean ± standard deviation ($\bar{x} \pm s$). Prior to statistical testing, normality (Shapiro-Wilk test) and homogeneity of variance (Levene's test) were assessed. For two-group comparisons, independent t-tests were applied to normally distributed data with equal variance, while non-normally distributed or unequal-variance data were analyzed using the Mann-Whitney U test. Multi-group comparisons employed one-way ANOVA with Ryan-Holm step-down Bonferroni post hoc tests for parametric data, whereas non-parametric data were evaluated via the Kruskal-Wallis H test followed by Dunn's post hoc analysis. All tests were two-tailed, with $P < 0.05$ considered statistically significant. Experiments included ≥ 3 biological replicates per group and were independently repeated three times to ensure robustness.

Discussion

PCa, a critical threat to global male health, continues to face therapeutic challenges, particularly in managing CRPC. This study is the first to systematically elucidate the molecular mechanisms by which the HDH-SBH drug pair suppresses PCa via the apoptosis signaling pathway, integrating network pharmacology, molecular docking, molecular dynamics simulations, and in vitro validation, thereby providing a scientific foundation for modernizing traditional Chinese medicine research. Beyond the mechanistic details elucidated herein, the HDH-SBH drug pair finds its rationale in the clinical practice of TCM for cancer management, often as an adjunct therapy to ameliorate side effects of conventional treatment and potentially delay resistance. Our findings provide a molecular footing for these clinical observations. The simultaneous downregulation of the anti-apoptotic protein BCL2 and the inflammatory transcription factor p-65 by HDH-SBH components suggests a concerted strategy to dismantle two critical pillars of cancer cell survival: resistance to cell death and inflammation-driven proliferation. This multi-target attack is particularly relevant for CRPC, which is notorious for its dependency on alternative survival pathways that bypass androgen signaling. The observed suppression of AKT1 phosphorylation further underscores the ability of HDH-SBH to intercept a master regulator of oncogenic signaling. Therefore, the HDH-SBH drug pair represents a promising multi-pronged therapeutic approach rather than a single-target inhibitor.

Recent advancements highlight TCM's unique advantages in oncology, particularly in reversing drug resistance and modulating the tumor microenvironment. Our findings demonstrate that HDH-SBH drug pair inhibits PC-3 cell proliferation, migration, and survival through multi-component interactions. Network pharmacology identified quercetin, ursolic acid, and apigenin as core active components targeting key nodes (AKT1, BCL2, NFKB) within the apoptosis pathway. These results align with prior studies: quercetin induces apoptosis in PC-3 cells by inhibiting the PI3K/AKT pathway[21]; ursolic acid activates caspase cascades in cholangiocarcinoma models[22]; and apigenin upregulates caspase-8, caspase-3, and TNF-α to suppress cancer stem cell proliferation[23]. Molecular docking and dynamics simulations further validated stable binding between these components and their targets, with apigenin-AKT1 exhibiting the highest stability, suggesting its pivotal role in HDH-SBH's anti-PCa efficacy. Importantly, given the multi-component, multi-target nature of HDH-SBH, its efficacy likely arises from a network-wide perturbation rather than the inhibition of a single target. Our integrated approach, combining network pharmacology prediction with rigorous molecular dynamics simulations that demonstrated stable ligand-target interactions over 100 ns, provides strong in silico evidence for the engagement of these core targets. The subsequent in vitro validation, showing consistent downregulation at both mRNA and protein levels of this target axis (AKT1 phosphorylation, BCL2, p-65) alongside the functional outcome of apoptosis induction, offers a coherent line of evidence supporting our proposed mechanism. Direct genetic perturbation of these key nodes, while insightful, could be confounded by complex feedback loops and compensatory mechanisms within the highly interconnected apoptosis network. Therefore, we posit that our current multi-faceted methodology provides a robust and systems-level substantiation of the mechanism. We acknowledge that siRNA/knockdown experiments represent a definitive future step to further refine the model, particularly in delineating the individual contribution of each target, and we have included this as a key perspective in the conclusion. It is important to note that this study utilized the PC-3 cell line, which is a well-established model for aggressive, CRPC[24]. The selection of PC-3 cells was intentional, as our research focuses on elucidating therapeutic strategies for the challenging CRPC stage, where androgen-responsive therapies often fail. While investigating the effects on androgen-responsive cell lines and normal prostate epithelial cells would provide a broader perspective, the primary objective here was to dissect the mechanism in a model representative of treatment-resistant disease.

KEGG enrichment pinpointed the apoptosis pathway as HDH-SBH's central mechanism, corroborated by in vitro experiments showing downregulated BCL2 and p-65 (NF-κB subunit) protein expression alongside increased AKT1 phosphorylation (p-AKT1/AKT1 ratio). This apparent paradox may reflect multi-target regulation: suppressed AKT phosphorylation could suppress downstream pro-survival signals via negative feedback[25], while BCL2 downregulation directly weakens anti-apoptotic defenses. The p-65 inhibition further suggests disruption of inflammation-driven survival signals in the tumor microenvironment[26]. Such multi-target synergy epitomizes TCM's principle of Zeng Xiao Jian Du (enhanced efficacy, reduced toxicity). Notably,

repeated attempts to detect p-p-65 via Western blot were unsuccessful, likely due to its low baseline expression in PC-3 cells.

The scratch assay revealed time-dependent inhibition of PC-3 cell migration by HDH-SBH drug pair, with a 64.23% reduction at 36 h, potentially linked to NF-κB-mediated suppression of MMP-9[27]. Flow cytometry confirmed significant apoptosis induction (13.57% vs. 4.79%), aligning with KEGG predictions and validating HDH-SBH's pro-apoptotic effects.

Innovatively, this study introduced molecular dynamics simulations to TCM research, demonstrating that the AKT1-apigenin complex maintained stable RMSD values (~ 4.8 Å) and 2–6 hydrogen bonds over 100 ns simulations, atomically resolving binding stability. This computational-experimental paradigm offers a methodological framework for deciphering multi-component synergism in herbal medicine[25]. This study has several limitations. The exclusive use of PC-3 cells may not fully capture PCa heterogeneity, and the absence of in vivo data limits pharmacokinetic and safety profiling. Furthermore, while our UPLC-Q/TOF-MS analysis successfully identified key active components and in vitro assays demonstrated significant biological effects at the tested concentrations (IC_{50} = 1.094 mg/mL), we acknowledge that directly extrapolating our extract concentration to the clinical dosage of raw herbs requires caution. The therapeutic efficacy of TCM, however, often arises from the synergistic interplay of multiple components rather than the abundance of a single compound. The identified components, even at relatively low individual concentrations, can collectively exert potent effects by targeting multiple nodes within a biological network, as demonstrated by our systems pharmacology and experimental results[28]. Future studies should employ quantitative mass spectrometry to precisely determine the concentrations of these active components in the extract and correlate them with pharmacological activity. Additionally, future studies aimed at quantifying the plasma and tissue levels of these key components after administration of the HDH-SBH decoction, and exploring formulation strategies to enhance their bioavailability, will be critical steps in bridging the gap between our mechanistic findings and clinical application for PCa therapy.

Conclusion

This study confirms that the HDH-SBH drug pair targets AKT1, BCL2, and NFKB to regulate the apoptosis signaling pathway, inhibiting PC-3 cell proliferation and inducing apoptosis. These findings not only provide experimental evidence for TCM in PCa treatment but also establish a systems pharmacology framework for modernizing complex herbal formulations. A limitation of this work is the focus on a single, androgen-independent cell line, and future investigations will be strengthened by including both androgen-responsive and normal prostate cell lines to fully assess the therapeutic window and spectrum of efficacy of HDH-SBH. Furthermore, while our data strongly implicate the identified target axis, genetic knockdown studies would be a valuable next step to conclusively define the dependency of the observed effects on each individual target within this network. This study lays the necessary groundwork for such future in-depth mechanistic explorations.

Data availability

The data that support the findings of this study are available from the corresponding author upon reasonable request.

Received: 22 August 2025; Accepted: 12 December 2025
Published online: 17 December 2025

References

1. Siegel, R. L., Miller, K. D., Fuchs, H. E. & Jemal, A. Cancer statistics, 2022. *CA Cancer J. Clin.* **72**(1), 7–33 (2022).
2. Filho, A. M. et al. The GLOBOCAN 2022 cancer estimates: data sources, methods, and a snapshot of the cancer burden worldwide. *Int. J. Cancer*. **156**(7), 1336–1346 (2025).
3. Feng, R. M., Zong, Y. N., Cao, S. M. & Xu, R. H. Current cancer situation in china: good or bad news from the 2018 global cancer statistics. *Cancer Commun. (Lond)*. **39**(1), 22 (2019).
4. Vis, D. J. et al. Whole genome sequencing of 378 prostate cancer metastases reveals tissue selectivity for mismatch deficiency with potential therapeutic implications. *Genome Med.* **17**(1), 24 (2025).
5. Guo, Y. et al. Wnt5a augments intracellular free cholesterol levels and promotes castration resistance in prostate cancer. *J. Transl Med.* **23**(1), 347 (2025).
6. Wang, L. Y. et al. PROTACs as therapeutic modalities for drug discovery in Castration-Resistant prostate cancer. *Annu. Rev. Pharmacol. Toxicol.* **65**(1), 375–396 (2025).
7. Zhang, X., Qiu, H., Li, C., Cai, P. & Qi, F. The positive role of traditional Chinese medicine as an adjunctive therapy for cancer. *Biosci. Trends*. **15**(5), 283–298 (2021).
8. Yuan, J. et al. Traditional Chinese medicine for breast cancer treatment: a bibliometric and visualization analysis. *Pharm. Biol.* **62**(1), 499–512 (2024).
9. Zou, Y. et al. The triangular relationship between traditional Chinese medicines, intestinal flora, and colorectal cancer. *Med. Res. Rev.* **44**(2), 539–567 (2024).
10. Zhang, R. et al. Isolation, purification, structural characteristics, Pharmacological activities, and combined action of Hedyotis diffusa polysaccharides: A review. *Int. J. Biol. Macromol.* **183**, 119–131 (2021).
11. Zheng, Q., Wu, X. & Peng, S. The immunotherapy mechanism of Hedyotis diffusae herba in treating liver cancer: a study based on network pharmacology, bioinformatics, and experimental validation. *Naunyn Schmiedebergs Arch. Pharmacol.* **398**(1), 951–965 (2025).
12. Wang, C. Y. et al. Effect of Chinese herbal medicine therapy on overall and cancer related mortality in patients with advanced nasopharyngeal carcinoma in Taiwan. *Front. Pharmacol.* **11**, 607413 (2020).
13. Shao, H. et al. Salvigenin suppresses hepatocellular carcinoma Glycolysis and chemoresistance through inactivating the PI3K/AKT/GSK-3β pathway. *Appl. Biochem. Biotechnol.* **195**(8), 5217–5237 (2023).
14. Wang, S. et al. Compatibility Art of traditional Chinese medicine: from the perspective of herb pairs. *J. Ethnopharmacol.* **143**(2), 412–423 (2012).
15. Wu, L. et al. Application of network Pharmacology and molecular Docking to elucidate the potential mechanism of Astragalus-Scorpion against prostate cancer. *Andrologia* **53**(9), e14165 (2021).

16. Wu, L. et al. Exploring the mechanism of action of sparganii rhizoma-Curcumae rhizoma for in treating castration-resistant prostate cancer: a network-based Pharmacology and experimental validation study. *Sci. Rep.* **14**(1), 3099 (2024).
17. Miao, W. G., Tang, C., Ye, Y., Quinn, R. J. & Feng, Y. Traditional Chinese medicine extraction method by ethanol delivers drug-like molecules. *Chin. J. Nat. Med.* **17**, 713–720. https://doi.org/10.1016/S1875-5364(19)30086-X (2019).
18. Meng, W., Xiaoliang, R., Xiumei, G., Vincieri, F. F. & Bilia, A. R. Stability of active ingredients of traditional Chinese medicine (TCM). *Nat. Prod. Commun.* **4**, 1761–1776 (2009).
19. Jo, S., Kim, T., Iyer, V. G. & Im, W. CHARMM-GUI: a web-based graphical user interface for CHARMM. *J. Comput. Chem.* **29**(11), 1859–1865 (2008).
20. Mark, P. & Nilsson, L. Structure and dynamics of liquid water with different long-range interaction Truncation and temperature control methods in molecular dynamics simulations. *J. Comput. Chem.* **23**(13), 1211–1219 (2002).
21. Jia, B. et al. 6-C-methylquercetin in Baeckea frutescens exerts anti-prostate cancer effect via ErbB/PI3K/AKT pathway. *Phytomedicine* **139**, 156463 (2025).
22. Maphanao, P. et al. Synchrotron FTIR microspectroscopy revealed apoptosis-induced biomolecular changes of cholangiocarcinoma cells treated with ursolic acid. *Biochim. Biophys. Acta Gen. Subj.* **1864**(12), 129708 (2020).
23. Erdogan, S. et al. The flavonoid apigenin reduces prostate cancer CD44(+) stem cell survival and migration through PI3K/Akt/NF-κB signaling. *Life Sci.* **162**, 77–86 (2016).
24. Cabello, M. et al. Extracellular electrophysiology in the prostate cancer cell model PC-3. *Sens. (Basel)*. 19. https://doi.org/10.3390/s19010139 (2019).
25. Hammerich, K. H., Frolov, A., Li, R., Ittmann, M. & Ayala, G. E. Cellular interactions of the phosphorylated form of AKT in prostate cancer. *Hum. Pathol.* **63**, 98–109 (2017).
26. Zhu, G. et al. Exploring the multi-targeted mechanism of Saikosaponin A in prostate cancer treatment: a network Pharmacology and molecular Docking approach. *Front. Pharmacol.* **16**, 1530715 (2025).
27. Ha, S. H. et al. Esculentoside H inhibits colon cancer cell migration and growth through suppression of MMP-9 gene expression via NF-kB signaling pathway. *J. Cell. Biochem.* **120**(6), 9810–9819 (2019).
28. Wang, S. et al. Metabolic reprogramming by traditional Chinese medicine and its role in effective cancer therapy. *Pharmacol. Res.* **170**, 105728. https://doi.org/10.1016/j.phrs.2021.105728 (2021).

Author contributions

J. Q., L. W. and Z. H.: writing—original draft. Y. S., Y. W. and Q.W.: methodology. Z. C., W. C. and Q. Z.: formal analysis. X. Y. and W. Z.: writing–review & editing. All authors contributed to the article and approved the submitted version. All authors contributed to the conception and design of the study, interpretation of data, and critically revised the manuscript for important intellectual content. The authors confirm that no paper mill and artificial intelligence was used.

Funding

This work was supported by the Young Elite Scientists Sponsorship Program by CACM (Program no. 2023-QNRC2-A10), Guangdong Provincial Natural Science Foundation GeneralProject (Program no. 2024A1515012209), Shenzhen Bao'an Chinese Medicine Hospital Research Program (Program no. BAZYY20220703), 2024 High-quality Development Research Project of ShenzhenBao'an Public Hospital (Program no. BAGZL2024128) and China Postdoctoral Science Foundation (Program no. 2024M750265).

Declarations

Competing interests

The authors declare no competing interests.

Additional information

Supplementary Information The online version contains supplementary material available at https://doi.org/10.1038/s41598-025-32757-6.

Correspondence and requests for materials should be addressed to X.J.Y. or W.B.Z.